Bus Cabin Cooling:

Feasibility of a Turbulent Jet

Ben Halliwell

6th March 2024

TRL

This report was produced for the Modern Approaches in Fluids topic of the Advanced Topics module at the University of Bristol.

As per the assessment brief, the author will assume the role of a consultant for the Transport Research Laboratory (TRL), however, this report has no affiliation with the genuine Transport Research Laboratory ltd.

This work was carried out using the computational facilities of the Advanced Computing Research Centre, University of Bristol - http://www.bristol.ac.uk/acrc/.

Definitions of technical jargon and concepts can be seen in Appendix A and in the grey boxes.

Cover Image: © Unsplash / Mariana Alves

Executive Summary

A high-fidelity computational fluid dynamics study was conducted into the feasibility of directly cooling a bus driver's head using a turbulent jet situated in the centre of the steering wheel.

The properties of the jet were determined directly for an arbitrary nozzle diameter and exit velocity from the high-fidelity simulation and indirectly from lower-fidelity simulations using standard RANS closure models.

The temperature of the jet was modelled in post-processing using a direct relationship between the concentration of a simulated passive scalar introduced at the nozzle and the ambient temperature of 40°C.

Self-similarity of the jet was demonstrated for concentration, and consequently temperature. Therefore, the optimal nozzle diameter could be determined solely from a single high-fidelity simulation.

Achieving a safe air temperature of 32°C everywhere in the region representing the driver's head from an orthogonally positioned nozzle was deemed to be impractical due to size constraints. Instead, it is recommended this performance requirement be relaxed to *achieving a mean temperature of 32°C in the head region* with a jet angled directly at the driver.

Based on this more attainable requirement, it is recommended the new UK bus regulations dictate a:

- 22cm diameter nozzle,
- angled at 21° to the vertical axis of the steering wheel,
- with a volumetric flow rate of 0.2-1.1m^3/min at 21°C.

However, the current concept has a number of limitations, mainly related to its position in the steering wheel. Therefore, it is suggested that the feasibility other nozzle locations and/or multiple jets be investigated before committing to adopting the aforementioned recommendation.

Introduction

Maintaining a high level of concentration is critical for the driver of a vehicle, especially mass transit vehicles such as buses, as the potential consequences of reduced driver focus are severe for passengers and pedestrians. Elevated ambient temperatures can cause the driver to experience heat stress which is known to cause a deterioration in cognitive performance. A study into the effect of heat on bus drivers suggested that the safe driving time, before the core temperature of the driver exceeds 38°C, at an ambient temperature of 40°C is approximately 50 minutes, whereas at 32°C it is at least 80 minutes, and probably indefinitely (Dong, 2022).

In the UK, more road traffic accidents occur in the summer months of the year (Apx. B). This is surprising, as intuitively more accidents should happen in the adverse weather conditions and longer nights of the winter months. Therefore, the hypothesis that increased cabin temperatures impair a driver's performance is plausible. Direct cooling of a person's forehead has been shown to provide an improvement in cognitive performance in hot conditions (Gaoua & Racinais, 2011); therefore, injecting a cool jet of air at the driver's head may enhance their ability to drive effectively (Fig. 1).

This report will evaluate the feasibility of direct cooling of the driver's head, by performing a single high-resolution computational fluid dynamics (CFD) simulation and a thorough statistical analysis of the results. A single simulation is sufficient to define the optimal nozzle radius as an axisymmetric jet is self-similar, meaning the time-averaged cooling effect is solely dependent on the radius of the jet (Box 2). Multiple iterative simulations would necessitate a poorer resolution for a given computation time, and since this project was severely time-constrained, a single simulation was preferred.

Box 1: What is Turbulence?

Turbulence is characterised by chaotic, unsteady behaviour of swirling vortices, known as eddies, across a wide range of length scales, and is typically associated with a high Reynold's number:

$$\mathrm{Re} = \frac{\text{inertial force}}{\text{viscous force}} = \frac{\rho U L}{\mu}, \tag{1}$$

where ρ is the density, U and L are the characteristic velocity and length and μ is the dynamic viscosity. The eponym of this dimensionless number, Osborne Reynolds, also proposed a decomposition of the fluid flow field u into a time-averaged flow $\overline{u(x)}$ and the instantaneous random fluctuations $u'(x,t)$:

$$u(x,t) = \overline{u(x)} + u'(x,t). \tag{2}$$

This is known as Reynold's averaged Navier-Stokes or RANS. By definition, both the time-average of the fluctuations and time-derivative of the mean flow is zero: $\overline{u'(x,t)} = 0$ and $\partial\overline{u(x)}/\partial t = 0$.

Jet Simulation

To simulate the cooling performance of the jet, the MOBILE implicit large eddy simulation (LES) software was used on the University of Bristol's supercomputer, BlueCrystal 4. A 10cm diameter jet was virtually positioned at the centre of a 1m^3 cube, representing the centre of the driver's steering wheel in the bus cabin (Fig. 1). The cabin was rotated by 12° with air injected at 0.2m/s (~0.1m^3/min) and with an equal flow rate out of the porous membrane. It should be noted that impact of the driver on the flow, and buoyancy effects were not simulated. Based on anthropological data, in the UK, the 95th percentile largest male has a finger-to-elbow length of 508mm and a vertical-elbow-to-eye length of 567mm (Pheasant, 1982). The performance of the jet was evaluated in a 250x250x250 mm box around this point (head-box), with the eye level central in the box and with the elbow and box aligned (Fig. 1). The 95th percentile male was assumed to be the worst-case scenario, as shorter drivers would be closer to the nozzle and experience increased cooling. Given the limited time available for this project, a 512x512x512 (512^3) cubic element mesh was implemented as a compromise between fidelity and computation time. The 512^3 mesh gives a minimum resolvable eddy size of 3.9mm, larger than the smallest eddies

Fig. 1: Diagram of the setup implemented in simulation.

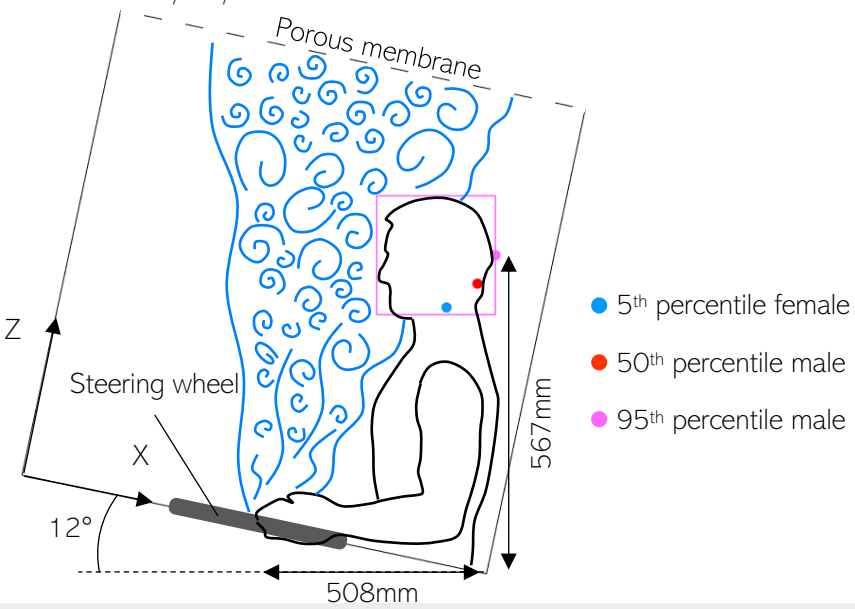

Box 2: Axisymmetric Turbulent Jets

An axisymmetric turbulent jet injected into a quiescent (stationary) fluid is a canonical example of free turbulence. An interesting quirk of a turbulent jet is that while momentum is conserved in the jet, mass flow increases, because the jet entrains fluid from the surrounding. This causes the radius of the jet R to linearly increase with distance z:

$$R(z) = R_0 + \alpha z, \tag{3}$$

where α is the mass entrainment factor and R_0 is the nozzle radius (Lawrie, 2018). It can also be shown that a theoretical free jet is self-similar, such that the axial velocity $\overline{u_z}$ and concentration $\bar{\phi}$ profile normalised by the value at the centreline of the jet $\overline{u_z}$ are constant throughout the jet:

$$\frac{\overline{u_z}(\eta)}{\overline{u_{z,c}}} = \frac{\bar{\phi}(\eta)}{\overline{\phi_c}} = \frac{1}{(1+\lambda\eta^2)^2}, \quad \text{where } \eta = \frac{x}{R(z)}. \tag{4}$$

(~0.8mm) based on the Kolmogorov length scale (Apx. C). Using LES means eddies smaller than 3.9mm are indirectly simulated; for an implicit LES, the inherent numerical truncation error is used to simulate the smallest eddies. The 512^3 mesh required over 130 hours of computation time to produce just 30 seconds of simulated data, validating the decision not to use an even finer mesh.

The concentration of the passive scalar 'dye' representing cool air can be seen in Fig. 2. Initially, the relative motion of the moving jet and quiescent fluid causes a toroidal vortex

determined using linear regression, between Z = 0 to 0.8m to avoid the dispersion of the jet at the wall contaminating the data (Fig. 3a), giving a mass entrainment factor $\alpha = 0.17$ (Eq. 3). This agrees closely with a value of 0.183 from experimental data (Boguslawski, 1979). Fig. 3b shows how the time-averaged jet follows the predicted analytical curve: $\lambda = 1.64$ (Eq. 4), confirming that the time-averaged jet is indeed self-similar. As the jet is self-similar (Box 2), this simplifies the design process as the concentration of the jet solely depends on its geometry.

Fig. 2: Concentration of passive scalar in the XZ plane at the midpoint of the Y axis, Re ~ 1300. (a) After 3s the jet shows a toroidal vortex and Kelvin-Helmholtz instabilities. (b) After 10s the jet shows a large variation in eddy size.(c) At 15s the jet has reached a time-averaged stead-state.

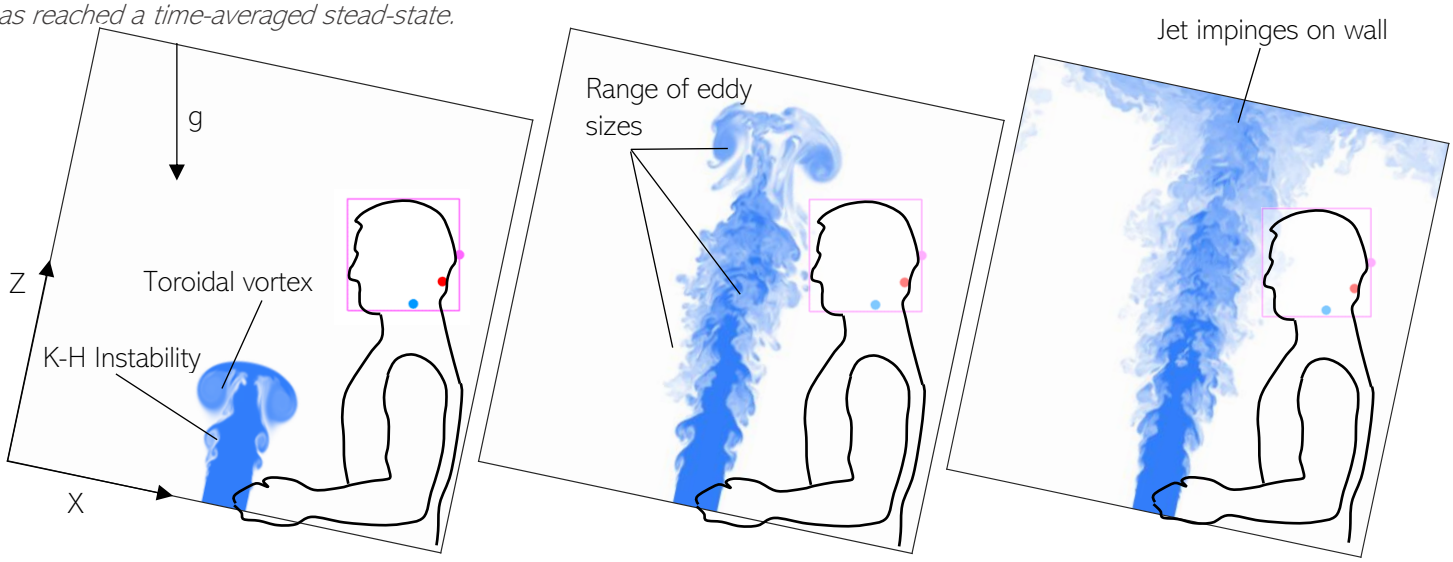

followed by Kelvin-Helmholtz instabilities, forming a range of different sized eddies, a quintessential characteristic of turbulence. Eventually, the jet impinges on the porous membrane, and henceforth, the time-averaged flow of the jet is steady. To reject the unsteady flow of the initial transient toroidal vortex (Fig. 2a), the average was taken from when the jet impinges on the wall (t = 11.5s) onwards.

Fig. 3a shows the time-averaged flow of the jet diverging linearly from a virtual origin around 0.3m below the jet exit. An inviscid potential core region forms in the centre of the jet and quickly dissipates into turbulence in the mixing regions either side of the core (White, 2006). The edges of the jet were defined as the points at which the passive scalar concentration was 10% of the maximum at that specific Z-displacement. The gradient of the jet was

Closure Models

To understand the turbulent properties of the jet beyond the analytical model, an axisymmetric numerical simulation was used. The radial diffusion of turbulence is analogous to molecular diffusion (Pope, 2001):

$$\frac{\partial \phi}{\partial t} = \frac{1}{r}\frac{\partial}{\partial r}\left(\nu_t r \frac{\partial \phi}{\partial r}\right). \qquad (5)$$

Two alternative methods of calculating the eddy viscosity ν_t (Box 3) of the jet were applied: the simple Modified Mixing Length (MML) (Prandtl, 1925) and more complex k-ε model (Launder & Spalding, 1983):

$$\nu_{t,MML} = \gamma UL, \qquad \nu_{t,k-\varepsilon} = C_\mu \frac{k^2}{\varepsilon}, \qquad (6)$$

Fig. 3: (a) Average dye concentration ϕ from 11.5 to 21 seconds at midpoint of Y axis for jet with nozzle radius R_0 = 5cm. (b) Self-similarity of the jet (dye concentration) at different Z-distances.

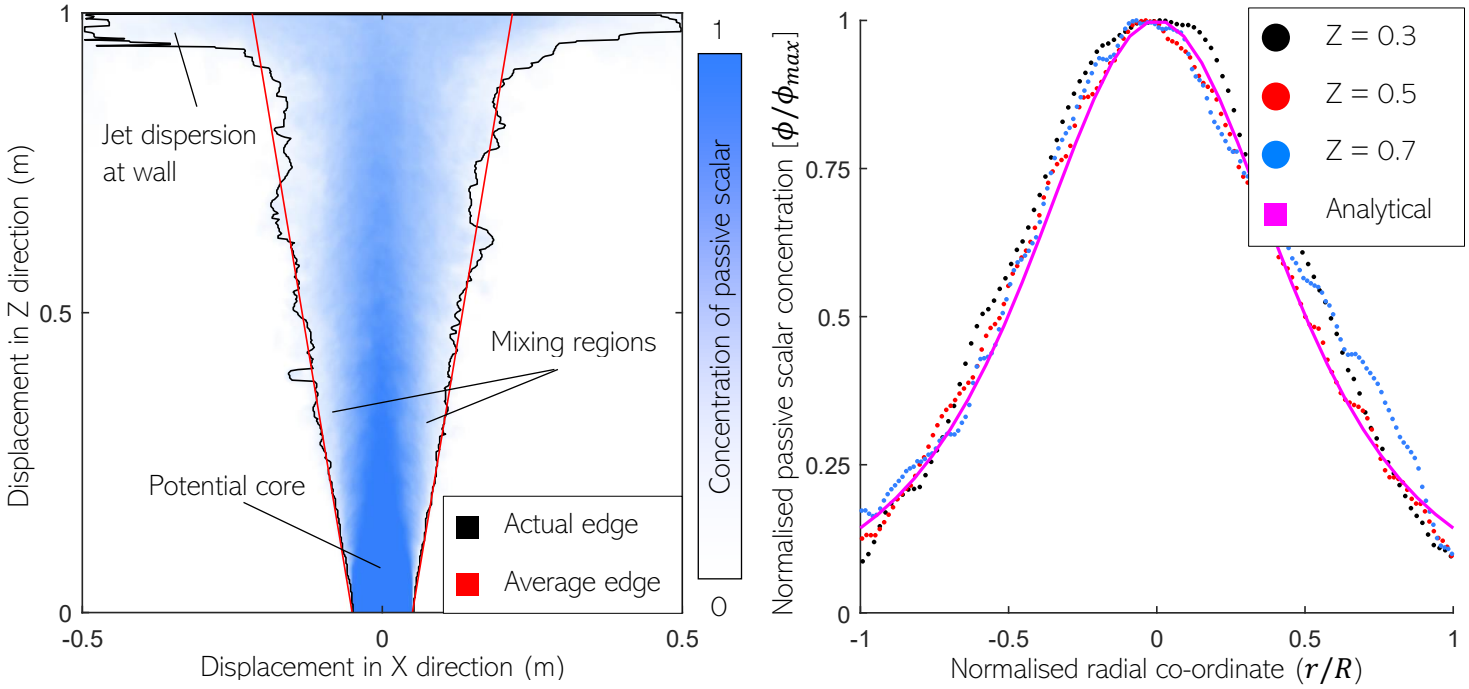

where γ and C_μ are constants, k is the turbulent kinetic energy (TKE) and ε is the turbulent energy dissipation (TED). The full mathematical and computational implementation of both models can be seen in Appendix D. The primary assumptions in the model were that the jet was steady-state, momentum was conserved, and that velocity only varied in the Z-direction. The turbulent diffusion and eddy viscosity equations were solved simultaneously using a variable-step, 1st order Forward Euler numerical integrator. The Forward Euler method is less accurate than higher order Runge-Kutta methods; however, as the expected results are expected to be approximately linear (Eq. 3), sufficient accuracy can be achieved with a simple solver. To decrease the computation time, the step size was adapted dynamically based on the local error in the system. The number of degrees of freedom was minimised for simplicity when fitting the model parameters, with only γ adjusted in the MML and $k_0(I)$ in the k-ε model, giving γ = 0.015 and the turbulent intensity I = 3.5%. This agrees with the literature, with γ = 0.016 for boundary layers and γ = 0.018 for plane jets (White, 2006). All other parameters in the k-ε model were kept as the standard values (Apx. D) (Launder & Spalding, 1983).

Box 3: The Closure Problem

One of the largest problems associated with the RANS equations is known as the closure problem. As the mean of the turbulent fluctuations is zero $\overline{u'} = 0$, multiple terms in the Navier-Stokes (NS) equations can be cancelled; however, the mean of the product of the fluctuations, known as Reynold's stress, is not zero $\overline{u'u'} \neq 0$, and cannot be cancelled. Subsequently, there are more unknown variables than equations, which is mathematically unsolvable. The Reynold's stress term could be re-substituted back into the NS equations; however, this simply gives a higher order unknown $\overline{u'u'\frac{\partial u'}{\partial x}} \neq 0$. Continuing to follow this process only creates higher and higher order unknowns, without ever removing the unknown and closing the equations.

Therefore, in 1877 Boussinesq proposed an additional equation to calculate the Reynold's stress based on the viscous effect of small-scale eddies, known as the eddy viscosity ν_t (Pope, 2001).

The mixing length model shows better correlation with the LES jet profile (Fig. 4a), as γ was adjusted specifically to fit the radial profile, whereas I also needed to satisfy the TKE profile (Fig. 4c). The mass entrainment factors for both models are reasonably accurate, giving a time-averaged α of 0.24 and 0.22 for the MML and k-ε model respectively (Fig. 4b) compared to 0.17 from the LES. Both models predicted the mean axial velocity accurately (Fig. 4d); however, this is the time and radially averaged velocity. The assumption of a constant velocity across the jet is weak, as the LES shows a large variation in velocity across the jet. Therefore, the two closure models cannot estimate the variation in the rate of turbulent mixing across the jet, such as in the potential core versus in the mixing region (Fig. 3a), which is one of the major limitations of this simple model. The TKE in the k-ε model has a similar average gradient to that of the LES, although the initial TKE is significantly higher (Fig. 4c). It is known that the standard k-ε model does not predict axisymmetric jets well (Launder & Spalding, 1983), so the inaccuracy in the k-ε predictions is expected.

Fig. 4: Comparison of steady-state LES and closure models (a) radii, (b) mass entrainment factor, eddy viscosity and (c) mean axial velocity. (d) Comparison of the turbulent kinetic energy at t = 21s for LES and steady-state for k-ε model. The order of labelling is clockwise starting from top left.

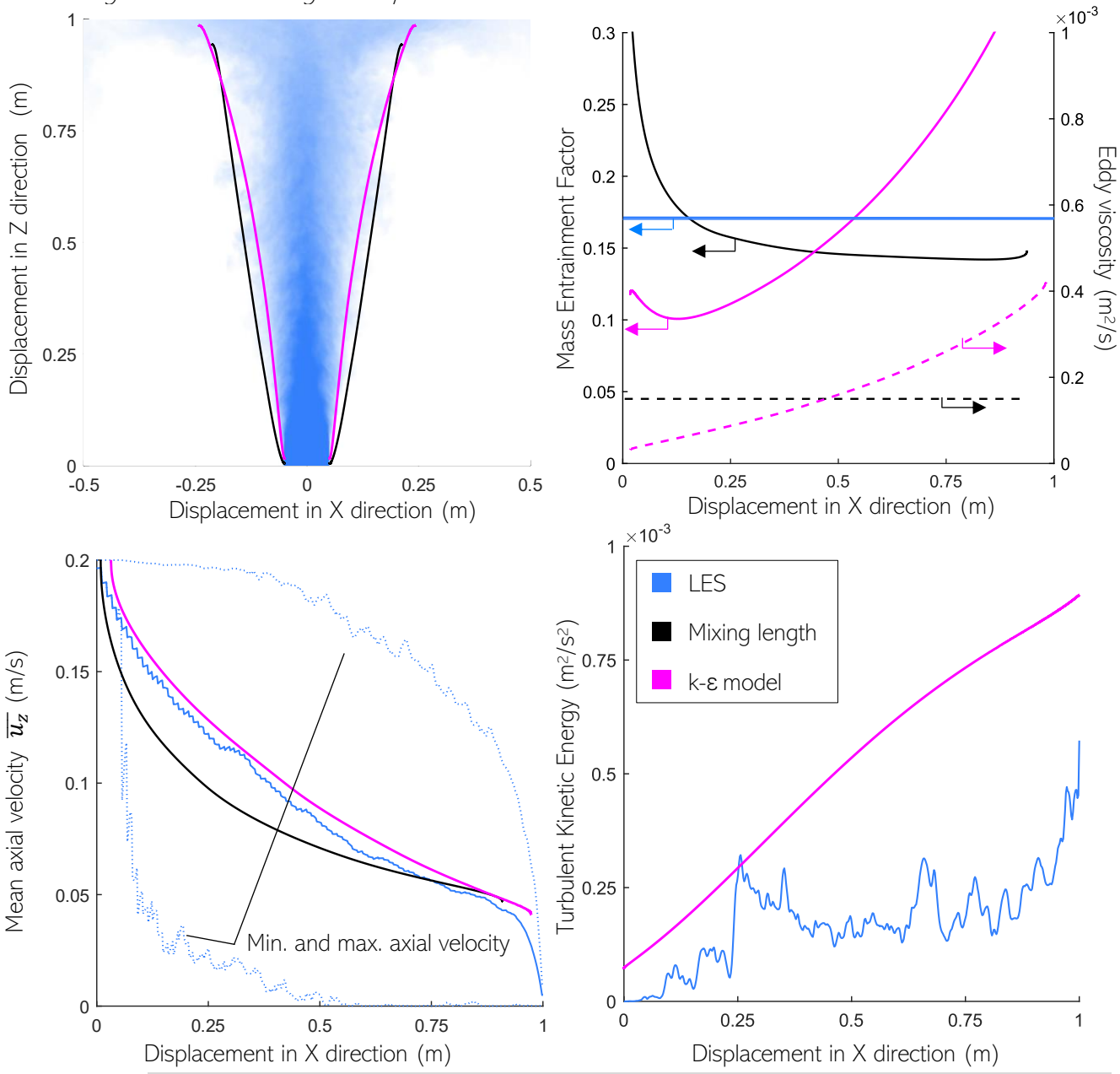

Heat Transfer

If the variation in temperature is small, it can be assumed the temperature has no effect on the flow (Pope, 2001), and therefore a passive scalar can be used to model the temperature T:

$$T = T_{amb} + (T_{jet} - T_{amb})\phi(r,z), \quad (7)$$

where T_{amb}=40°C and T_{jet}=21°C are the temperatures of the hot ambient and cool injected air respectively. Fig. 5 shows a limited cooling effect of the jet in orthogonal 2D planes at the side and centre of the cube representing the driver's head (head-box), with a minimum temperature of 33°C, above the safe temperature limit. This is because the jet bypasses the driver before exiting out of the porous membrane at the top. It was found that the entrainment factor was constant in the MML model or had a slight negative correlation with velocity in the k-ε model (Fig. 6a). For simplicity, the MML assumption that α = 0.17 is a constant was used. Thus, a nozzle of 0.37m (Fig. 1, Eq. 3) is required for the jet to encompass the entire headbox, and an even larger nozzle is required to ensure all of the head-box remains below 32°C, larger than the steering wheel itself.

Instead, the nozzle could be aimed directed at the driver, to minimise the cool air bypass. The jet itself was not rotated in simulation due to the extensive computation time required for a high-fidelity simulation, so the previous simulation was rotated by 21° to direct the jet at the centre of the head-box (Fig. 6b). As the walls have limited impact on the flow of the jet in the head-box, and since buoyancy effects were neglected, the rotation of the geometry and gravity vector was assumed to have minimal effect. Nonetheless, the 10cm diameter jet still provided insufficient cooling to the driver.

As the jet is self-similar (Fig. 3b), the temperature profile across the normalised radius is identical everywhere in the jet and can be used to predict the temperature across a larger jet. The maximum width of the head-box in the XZ plane occurs at Z = 0.7m and is 0.34m (Fig. 6b). However, the maximum width of the head-box in any plane is across the diagonal at 0.36m. The head-box is not axi-symmetric but if the radius of cool air (T<32°C) in the jet is greater than R_{H-B} = 0.18m at Z = 0.7m, then the entirety of the head-box will be sufficiently cooled.

Fig. 5: Performance of jet: R_0=5cm, based on orthogonal jet position in the (a) XZ plane at the side (Y = 125mm) and (b) YZ plane at the centre (X = 0mm) of the head box. In both cases the jet passes in front of the driver with minimal cooling effect.

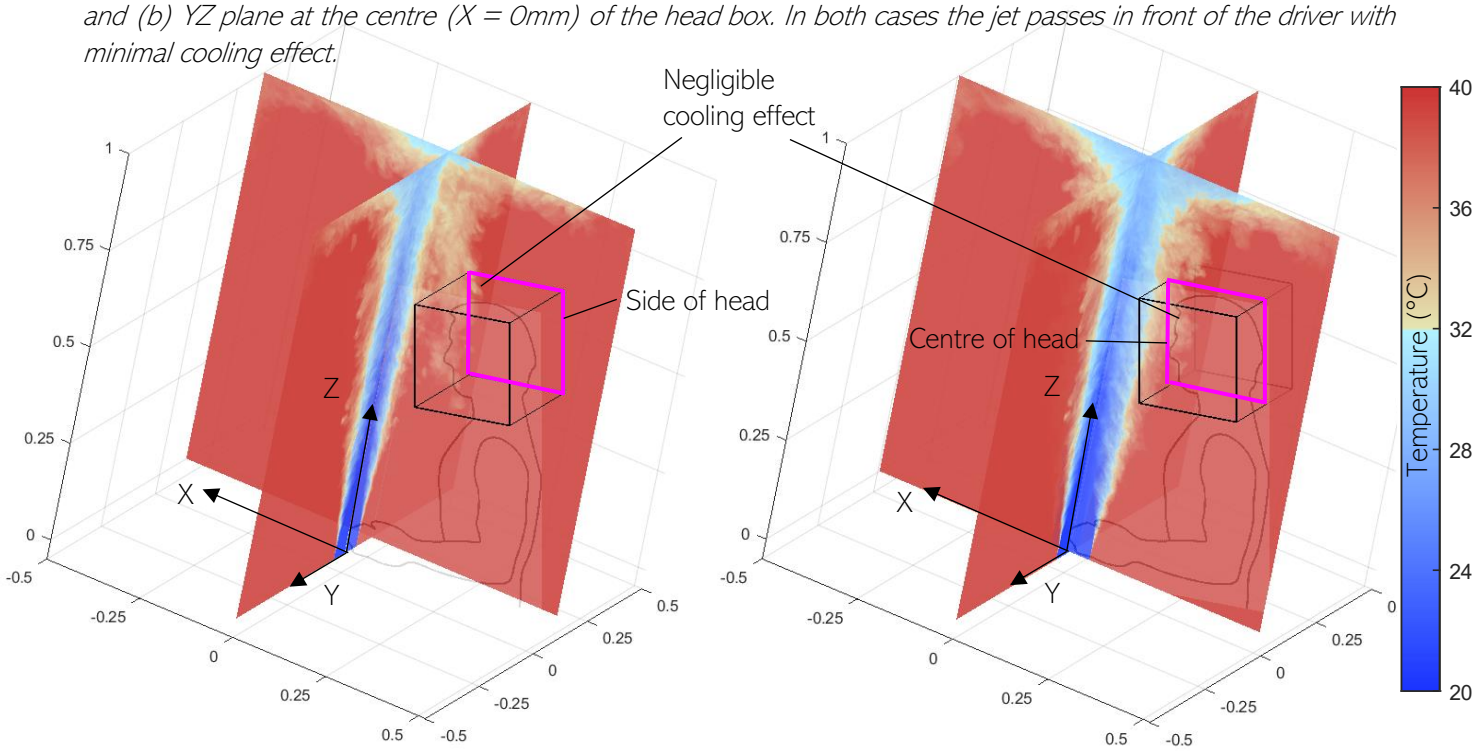

Fig. 6: (a) Impact of varying velocity on the radius of the jet. (b) Temperature in the XZ plane after rotating the jet by 21 degrees at the side of the head (Y = 125mm). The regions that would not be in a rotated simulation have been shaded.

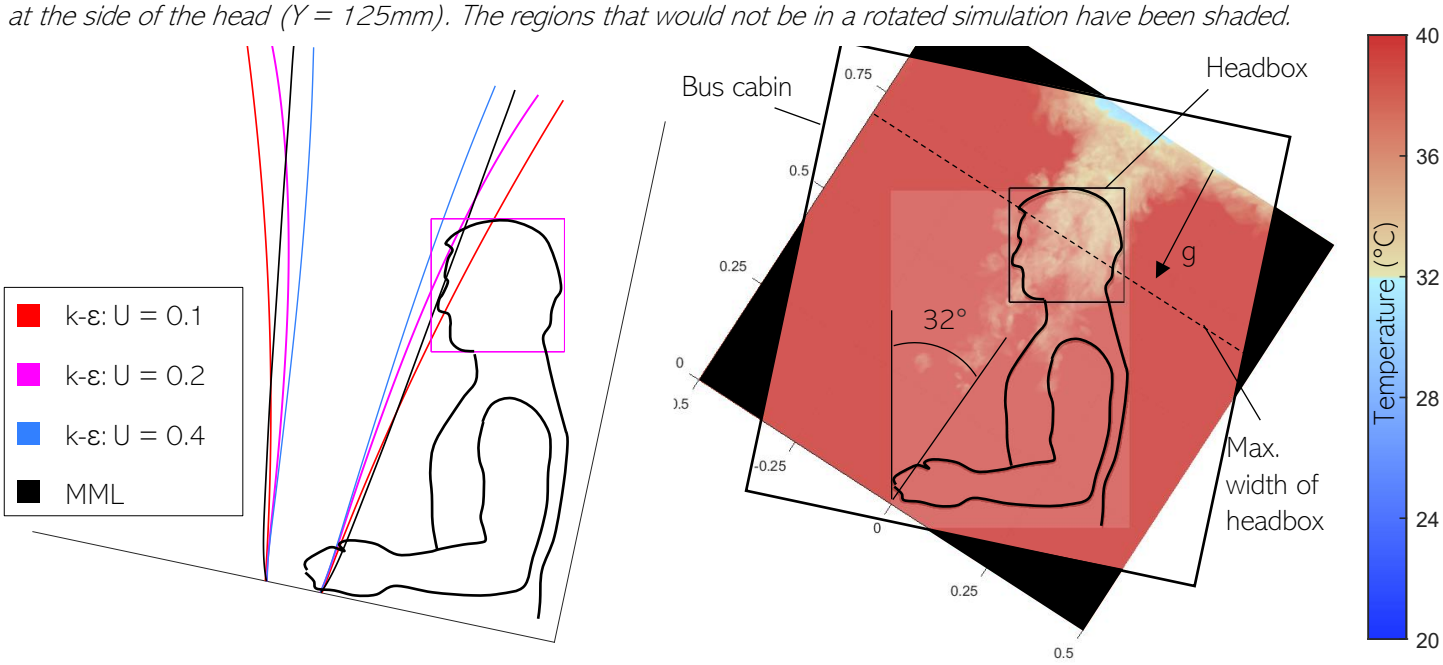

The time-averaged passive scalar concentration at the centre of the jet at Z = 0.7m was ϕ_{max} = 0.71; however, the instantaneous concentration fluctuates wildly. Therefore, to ensure 95% certainty, the time-averaged concentration was reduced by 2 standard deviations, giving 0.48 (Fig. 7a). ϕ_{max} can then be substituted into the self-similarity graph (Fig. 3b) and transformed into temperature (Eq. 7). The temperature self-similarity curve closely follows the time-averaged temperature data from the simulation; however, the 95% certainty curve does not (Fig. 7b). This is because the standard deviation not only changes ϕ_{max} but also the shape of the concentration distribution. To compensate, the shape distribution factor λ was increased to 3.1 (Eq. 4). This gives a normalised radius r/R = 0.22 for 95% confidence scenario.

Consequently, to ensure that nowhere in the head-box exceeds 32°C at any time once the jet has reached steady state with 95% confidence, the total radius of the jet must be

Fig. 7: (a) Decay of concentration of passive scalar along the centreline of jet. (b) Self-similarity of the temperature in the jet at Z = 0.7m, based on Figure 3b.

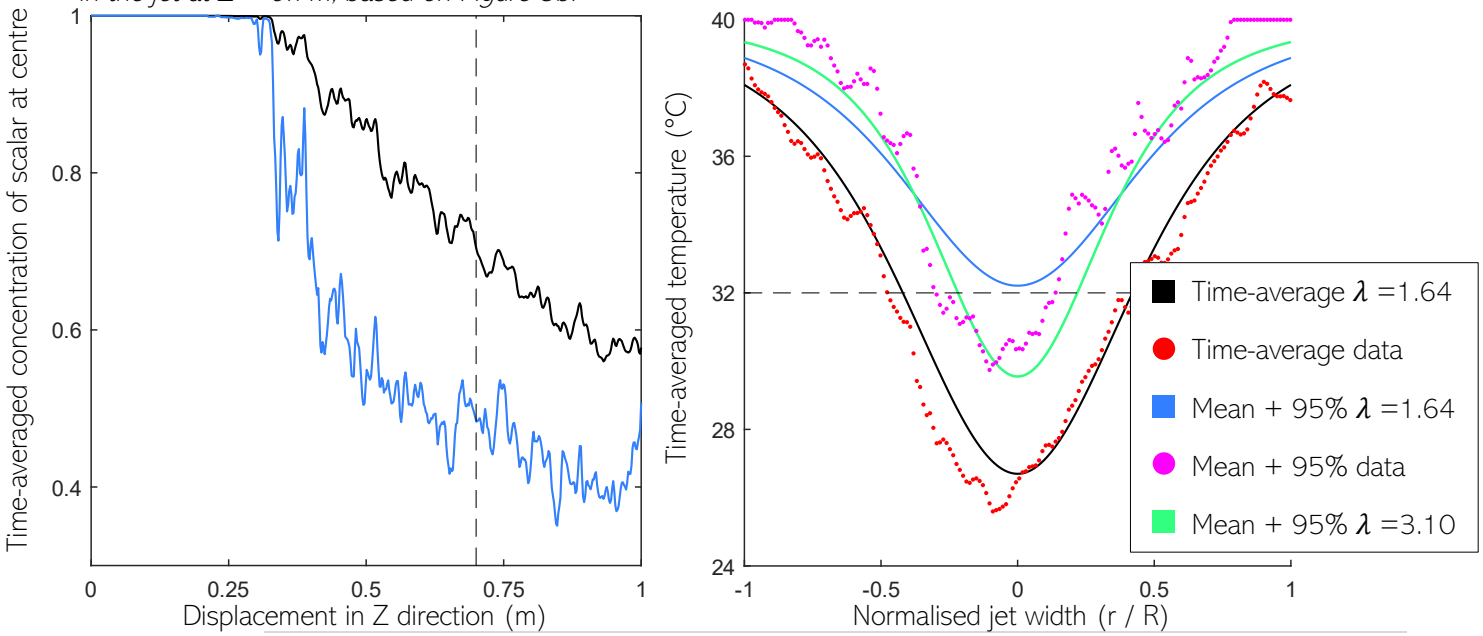

0.81m at Z = 0.7m. This is physically impossible given the width of bus cabin is 1m.

However, it should be questioned whether the entirety of the air in the head-box needs to be always kept below 32°C to ensure the driver's head remains below 32°C. Since the time-average of the fluctuations is zero (Box 1), the fluctuations which increase the temperature will be counteracted by those which decrease the temperature over a sufficiently long time. As the volume of the driver's head is much greater than that of the eddies, and thermal conduction through the driver's skin will occur faster than convection at the interface, these fluctuations will have a negligible effect on the temperature of the driver's head, and therefore specifying that nowhere in the head-box should ever exceed 32°C is excessively stringent.

Instead, a time-averaged temperature of 32°C is more reasonable. To ensure that nowhere in the headbox (R_{H-B}=0.18m) has a time-averaged temperature above 32°C, r/R = 0.42 (Fig. 7b) giving the total radius of the jet as 0.43m at Z = 0.7m. This is physically possible; however, the nozzle radius must be 0.29m with α = 0.17 (Eq. 3), which is infeasible to implement as the nozzle would be larger than the width of the steering wheel. Therefore, even with a jet directed at the driver, it is infeasible to ensure a safe average temperature everywhere in the head-box.

A further relaxation to this requirement is necessitated. Since the head-box is larger than the driver's head, if the direction of the jet is controllable, the driver could aim the cooler, central column of air at their head. Also, if the volume of the driver's head is considered, the actual volume of air in the headbox will be less than simulated and it will be the hot air at the boundary which is displaced. Finally, forced convection will occur at the interface between the driver's skin and the air, which will remove heat more effectively than free convection.

Therefore, rather than maintaining a safe time-average temperature everywhere in the head-box, it is argued that it is sufficient to maintain a time-average of 32°C averaged across the volume of the head-box. The normalised radius that achieves this is r/R = 0.64 (Fig. 7b) giving a more obtainable jet radius of 0.28m at Z = 0.7m and thus a nozzle of radius of 11cm.

After activating the jet, the driver will notice the cooling effect 5 seconds later, as the initial transient vortex enters the head-box, followed by a decrease in temperature until steady state (Fig. 8b). Increasing the initial jet velocity will reduce this time and improve the rate of forced convection heat transfer that occurs; however, if

Fig. 8: (a) Performance of optimal diameter jet: R_0=11cm, based on 21° angled nozzle with 256³ mesh in the (a) XZ plane at the side (Y = 125mm) and (b) YZ at the front (X = -125mm) of the head box. (b) Spatial average across headbox over time.

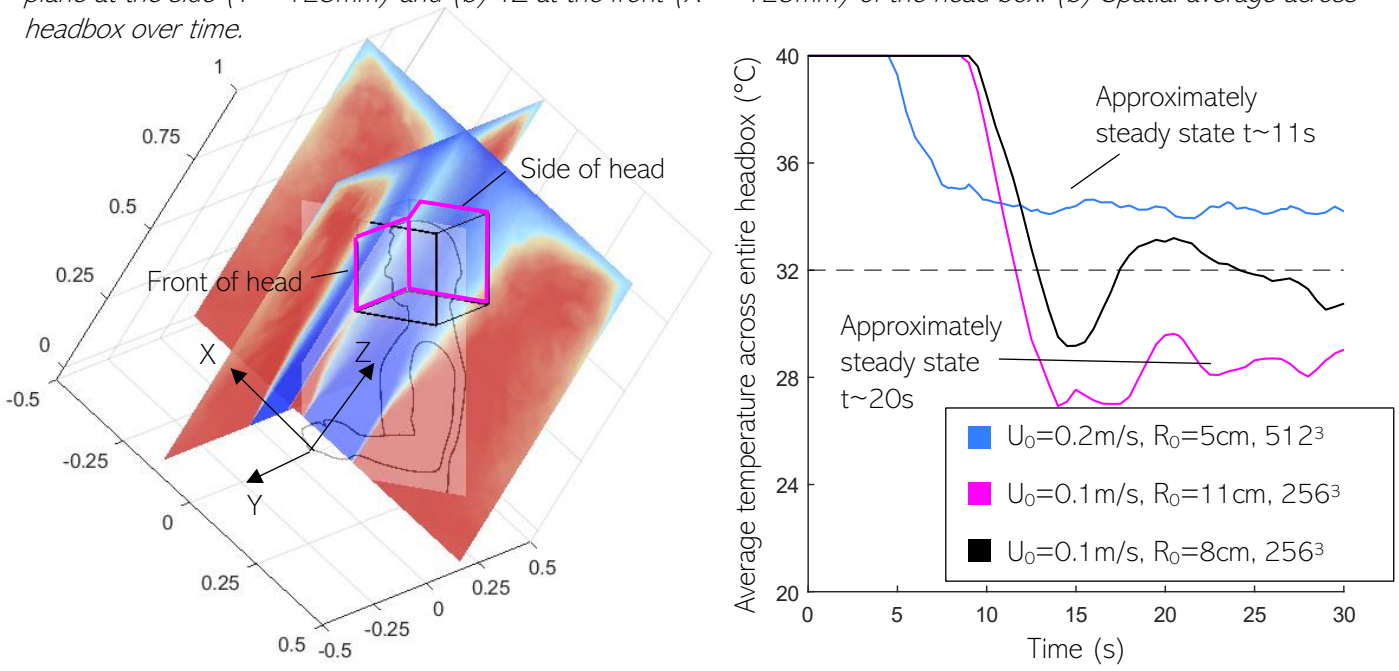

the velocity is too great, it could be distracting for the driver and would require a larger fan. The preferred option would be to enable the driver to control the velocity, in the range of ~0.1-0.5m/s which would achieve a steady-state temperature in 5-20 seconds.

Unfortunately, due to time constraints it was not possible to perform a second 512^3 element simulation. However, a 256^3 element simulation was performed with $U_0 = 0.1$m/s and $R_0 = 11$cm (Fig. 8a). The cooling of the jet performed better than self-similarity prediction with a time-average of 28.2°C across the entire head-box, albeit with an increased temperature fluctuation (Fig. 8b). It improved so much that even with $R_0 = 8$cm, a safe air temperature could be achieved. However, this is almost certainly caused by a 256^3 element simulation having an unrealistically high mass entrainment factor of up to 0.20 (Apx. E). This validates the earlier decision not to perform multiple 256^3 element simulation and a more conservative nozzle diameter of 22cm is still recommended.

Unfortunately, the jet still has numerous inherent design flaws. Placing the jet in the steering wheel will remove space for other components which are already located there, such as an airbag and horn. Additionally, the jet would protrude out of the steering wheel and become a hazard in an emergency braking event. These issues counteract the fundamental premise of the jet: to improve safety. Additionally, incorporating a non-rotating nozzle into the rotating steering wheel would increase design complexity and therefore cost, ultimately increasing bus fares for commuters.

Conclusion

Using a high-fidelity fluid dynamics simulation, it has been shown that achieving the safe temperature of below 32°C always and everywhere in the head-box is unrealistic given the inherent chaotic nature of turbulent flows. However, it is reasonable to achieve a spatio-temporal averaged temperature of 32°C. Based on this relaxed performance criteria, it is recommended the regulations specify a 22cm diameter jet, with an exit velocity of 0.1-0.5 m/s, for a volume flow rate of 0.2-1.1 m^3/min for the specified inlet temperature of 21°C.

Further analysis should be conducted into validating this design using a 512^3-element simulation or experimental methods. Studies should also be conducted into the feasibility of reducing the inlet air temperature or increasing the turbulence intensity in the nozzle, as this would allow a smaller diameter to nozzle to be used, as a 22cm diameter nozzle would still cause size related design challenges. It is also recommended that the feasibility of alternative or multiple jet positions are studied, as placing the jet at the centre of the steering wheel introduces safety concerns and design complexities. Finally, the simulation could incorporate more anthropomorphic elements, such as simulating the flow around the driver's head and the temperature of the driver's head, rather than the locally surrounding air.

References

Boguslawski, L. a. (1979). Flow structure of the free round turbulent jet. *Journal of Fluid Mechanics, 90*(3), 531-539.

Department for Transport. (2022). RAS9103: Reported casualties by police force, Great Britain, ten years up to 2022 (annual provisional estimates). Retrieved from https://www.gov.uk/government/statistical-data-sets/ras45-quarterly-statistics

Dong, X. S. (2022). Stress Response and Safe Driving Time of Bus Drivers in. *International Journal of Environmental Research and Public Health*. Retrieved from https://doi.org/10.3390/

Gaoua, N., & Racinais, S. (2011). Alterations in cognitive performance during passive hyperthermia. *International Journal of Hyperthermia*. Retrieved from https://doi.org/10.3109/02656736.2010.516305

Launder, B. E., & Spalding, D. B. (1983). The numerical computation of turbulent flows. *Numerical prediction of flow, heat transfer, turbulence and combustion.*, 96-116.

Lawrie, A. (2018). *Submerged Turbulent Jets.*

Pheasant, S. (1982). Anthropometric estimates for British civilian adults. *Ergonomics, 25*(11).

Pope, S. (2001). Turbulent Flows. 93,161.

Prandtl, L. (1925). 7. Bericht über Untersuchungen zur ausgebildeten Turbulenz. *ZAMM-Journal of Applied Mathematics and Mechanics/Zeitschrift für Angewandte Mathematik und Mechanik*, 136-139.

White, F. (2006). *Viscous Fluid Flow* (3 ed.). New York: McGraw-Hill.

Appendices

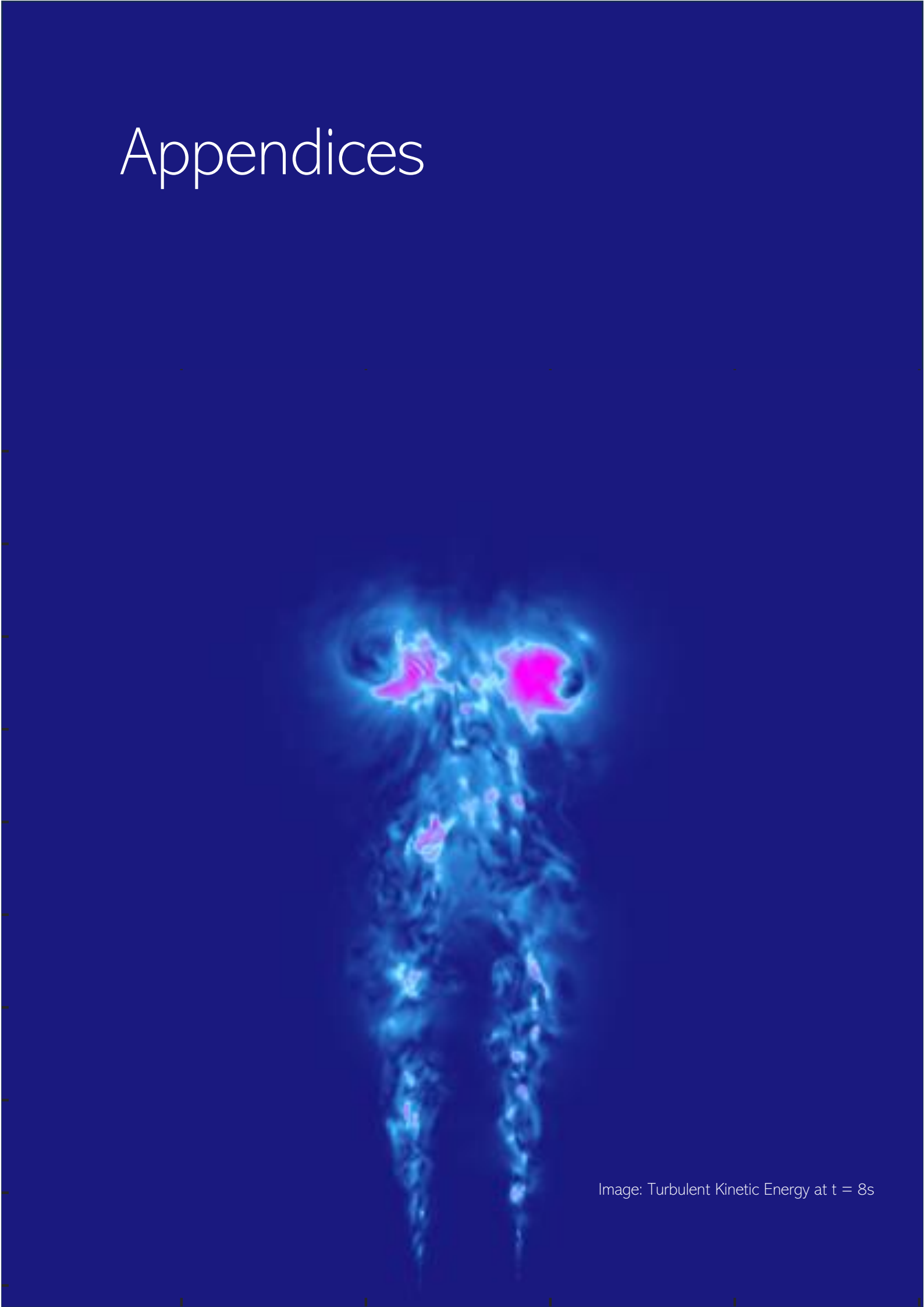

Image: Turbulent Kinetic Energy at t = 8s

Appendix A: Glossary

Axisymmetric – A geometry which has a rotational symmetry about an axis, such as a cylinder or sphere.

Canonical – A widely-studied and representative example (of turbulence).

Eddy – A swirling motion that occurs in a fluid.

Eddy viscosity – An effective viscosity which characterises the impact of small-scale eddies on the larger flow field.

Entrain – The phenomena by which a moving fluid incorporates another fluid as it flows past.

Head-box – The 250x250x250mm cube which encloses the driver's head, based on the height of the 95th percentile UK male.

Impingement – The collision of a fluid stream with a solid surface.

Kolmogorov length scale – The size of the smallest eddies.

Linear Regression – A method by which a straight line is chosen to be as similar as possible to the underlying data to minimise the difference between the datapoints and the line.

Passive scalar – A contaminant which is transported by a fluid, but has no impact on the fluid itself.

Quiescent - Being at a state of rest.

Self-similarity – Used to describe a system where parts of different length scales appear identical when scaled to be the same size.

Spatio-temporal average – Taking an average across both time and space.

Steady-state – A condition where the properties of a system do not change with time.

Toroidal vortex – A swirling mass of fluid which has a doughnut-like geometry.

Truncation error – Error caused by approximating an infinite sum of mathematical operations by only considering a finite number of operations.

A^3 – describing the number of the grid elements in the simulation. For instance, a 512^3 mesh would have 512 boxes in each the horizontal, vertical and depth-wise direction in which the velocity of fluid in that box is specified.

CFD (Computational Fluid Dynamics)- the use of numerical algorithms to predict the properties of a fluid flow.

K-H (Kelvin-Helmholtz instability)- An instability that occurs at the interface between two relatively moving fluids.

LES (Large Eddy Simulation)- a CFD method in which the smallest turbulent eddies are not simulated directly, but indirectly using some form of model which acts within each grid element.

NS (Navier-Stokes) - The equations that govern the flow of fluids, based on the conservation of mass and momentum (and sometimes energy).

MML (Modified Mixing Length) – A turbulent closure model for the RANS equations, which states the eddy viscosity depends only on the characteristic velocity and length-scale of the fluid and a constant.

RANS (Reynold's-Averaged Navier-Stokes)- a CFD method in which the time-fluctuating velocity is not simulated directly, but indirectly using some form of closure model. It is generally quicker but less accurate than LES.

TED (Turbulent Energy Dissipation)- a measure of the rate of conversion of turbulent kinetic energy to thermal energy in the eddies.

TKE (Turbulent Kinetic Energy)- a measure of the energy stored in the system as the random motion of eddies.

Appendix B: UK Temperature

Fig. 9: Mean monthly road traffic accidents and mean temperature for 2016-2022, excluding 2020. This year is excluded due to national lockdown restrictions reducing the number of vehicles on the road. Data from (Department for Transport, 2022).

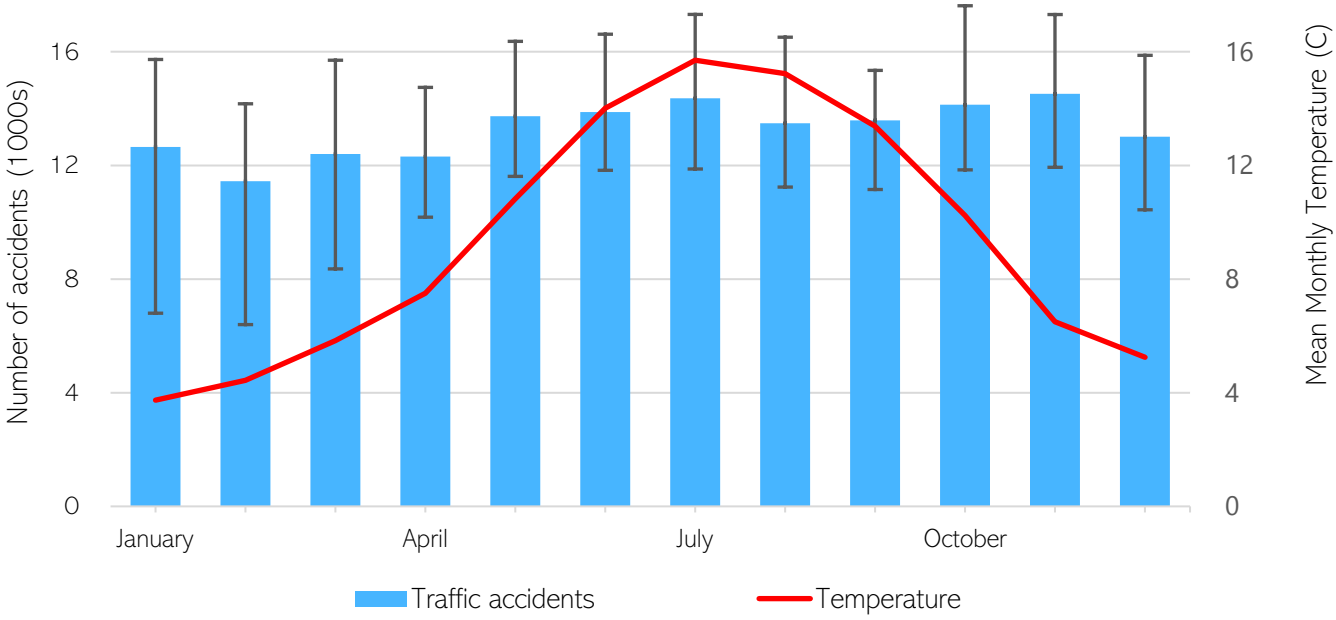

Appendix C: Kolmogorov Microscales

The Kolmogorov length scale η_L defines the smallest size of turbulent eddies before viscous forces dissipate the eddies into heat (Pope, 2001). The time scale η_t refers to the time it takes for this process to occur.

$$\eta_L = \left(\frac{\nu_t^3}{\varepsilon}\right)^{0.25}, \qquad \eta_t = \left(\frac{\nu_t}{\varepsilon}\right)^{0.5}. \quad (8)$$

From Fig. 4c, the minimum TKE away from the nozzle exit is ~1e-4 m²/s. From the numerical k-ε model, the largest TED was ~2e-4.

This gives a minimum eddy viscosity of ν_t ~ 4.5e-6 (Eq. 6) therefore η_L ~ 0.8mm, and η_t~0.15s. For comparison, the smallest eddy that can be resolved in simulation is a 2x2x2 cube of elements, which for the 512^3 simulation in a $1m^3$ box is ~4mm.

Appendix D: RANS Closure Modelling

D.1 Turbulent Diffusion

The turbulent diffusion of dye orthogonally to the flow of the jet can be expressed using Fick's 2nd law:

$$\frac{\partial \phi}{\partial t} = \frac{1}{r}\frac{\partial}{\partial r}\left(\nu_t r \frac{\partial \phi}{\partial r}\right), \qquad (9)$$

with the motion of the jet displacing the dye axially:

$$\frac{dz}{dt} = U_{jet}. \qquad (10)$$

As momentum is conserved: $AU_{jet}^2 = const,$ the velocity of the jet can be expressed in terms of the radius:

$$U_{jet}(z) = \frac{R_0}{R(z)} U_{jet,0}. \qquad (11)$$

Since the volumetric flow rate of the dye is constant, the total volume of dye at each z-level is also constant:

$$2\pi \int_{r=0}^{R} r\phi(r)dr = \phi_0 \pi r^2, \qquad (12)$$

which allows the radius of the jet to be solved.

D.2 Mixing Length Model

The simplest one equation model to estimate the eddy viscosity uses the principle that kinematic viscosity is dimensionally identical to the product of velocity and length. Taking the characteristic velocity and length as the axial jet velocity and radius respectively:

$$\nu_t = \gamma U_{jet} R. \qquad (13)$$

D.3 k-ε Model

However, the simplicity of the Prandtl mixing length model limits its effectiveness in predicting the turbulent characteristics. A more accurate method relates the eddy viscosity to the turbulent kinetic energy and dissipation:

$$\nu_t = C_\mu \frac{k^2}{\varepsilon}, \qquad (14)$$

Assuming the turbulent characteristics of the jet only vary in the axial direction, the k-ε transport equations can be simplified :

$$\frac{\partial k}{\partial t} = \frac{\partial}{\partial z}\left(\frac{\nu_t}{\sigma_k}\frac{\partial k}{\partial z}\right) + 2\nu_t\left(\frac{\partial U_{jet}}{\partial r} - \frac{k}{3}\right) - \varepsilon - U_{jet}\frac{\partial k}{\partial z} \qquad (15a)$$

$$\frac{\partial \varepsilon}{\partial t} = \frac{\partial}{\partial z}\left(\frac{\nu_t}{\sigma_\varepsilon}\frac{\partial \varepsilon}{\partial z}\right) + 2C_1\nu_t\left(\frac{\partial U_{jet}}{\partial r} - \frac{k}{3}\right)\frac{\varepsilon}{k} - C_2\frac{\varepsilon^2}{k} - U_{jet}\frac{\partial \epsilon}{\partial z}. \qquad (15b)$$

With C_μ = 0.09, σ_k = 1.0, σ_ε.=1.3, C_1=1.44, C_2=1.92. The standard initial conditions for k-ε are:

$$k_0 = \frac{3}{2}\left(U_{jet}I\right)^2, \ \varepsilon_0 = C_\mu^{\frac{3}{4}}\frac{k^{\frac{3}{2}}}{L_t}, \ L_t = \frac{7D_0}{100}, \qquad (16)$$

D.4 Numerical Implementation

To solve the diffusion equation, first order numerical differentiation was implemented:

$$\frac{\partial \phi}{\partial r} \approx \frac{\phi_{i+\frac{1}{2}} - \phi_{i-\frac{1}{2}}}{\Delta r}, \qquad (17)$$

With Dirichlet boundary conditions:

$$\phi_{i=0} = \phi_{i=end} = 0. \qquad (18)$$

The same process was repeated for terms inside the bracket. To numerically integrate, the 1st order Euler method was used due to its simplicity:

$$\phi_{n+1} = \phi_n + \frac{\partial \phi_n}{\partial t}\Delta t_n. \qquad (19)$$

To reduce the time required to calculate the answers, a variable time step was introduced. To determine the performance of the solver at each timestep, a full step (see above) and

double half-step numerical integration was performed:

$$\phi'_{n+1/2} = \phi_n + \frac{\partial \phi_n}{\partial t}\frac{\Delta t_n}{2}, \qquad (20)$$

$$\phi'_{n+1} = \phi_{n+1/2} + \frac{\partial \phi_{n+1/2}}{\partial t}\frac{\Delta t_n}{2}\ . \qquad (21)$$

Since the double half-step is assumed to always be more accurate than the single full-step, the effective error could be calculated:

$$e_{eff} = \left|\phi'_{n+1} - \phi_{n+1}\right|. \qquad (22)$$

This allowed the timestep to be dynamically adjusted based on a pre-determined error tolerance and saturation limits:

$$\Delta t_{n+1} = \min\left(\max\left(\sqrt{\frac{tol}{2e_{eff}}}, 0.5\right), 2\right)\frac{\Delta t_n}{1.01}. \qquad (23)$$

Additionally, simple moving average smoothing was applied to the concentration periodically to reduce the gradients which helped with reducing computation time. The radius of the jet was calculated by gradually increasing the test radius until the concentration exceeded 99.9% of the original concentration:

$$\text{while} \sum_{i=0}^{R_{test}} r\phi(i) < 0.999\frac{\phi_0 r^2}{2}, \quad R_{test} = R_{test} + 1. \qquad (24)$$

D.5 Computational Implementation (MATLAB)

D.5.1 Diffusion equation

```
function dphi_dt = diffusion_eq(r,dr,phi,k)

    % Calculate the rate of diffusion in radial co-ordinates

    % dphi/dr
    phi_half = [0 (phi(2:end) + phi(1:end-1))/2 0]; % Calculate the midpoints of
each element
    dphi_dr = diff(phi_half)/dr; % Calculate the 1st derivative

    % d/dr(kr_dphi_dr)
    kr_dphi_dr = k.*r.*dphi_dr;
    kr_dphi_dr_half = [0 (kr_dphi_dr(2:end) + kr_dphi_dr(1:end-1))/2 0];
    d_dr_kr_dphi_dr = diff(kr_dphi_dr_half)/dr;

    % Full equation
    dphi_dt = 1./r .* d_dr_kr_dphi_dr;

    % dividing by r = 0 gives NaN which must be removed by taking the
    % average of the co-ords either side
    nan_indx = find(isnan(dphi_dt));
    dphi_dt(nan_indx) = (dphi_dt(nan_indx-1) + dphi_dt(nan_indx+1))/2;
end
```

D.5.2 Smoothing function

```
function phi_new = smoothing(r,phi,i,freq,window)

    % Simple Moving Average smoothing
    % Occurs every *freq* iterations with window length *window_percent* %
    % of the entire spatial size

    centre_index = (length(r)+1)/2;
    if mod(i,freq) == 0 % every so often apply periodic smoothing
        phi2 = movmean(phi(centre_index:end),window);
        phi_new = zeros(1,length(r));
        phi_new(centre_index:end) = phi2;
        phi_new(1:centre_index) = fliplr(phi2);

        phi_tot = sum(phi .* abs(r)); % add a correction factor so the total
volume of dye does not change
        phi_tot_smooth = sum(phi_new .* abs(r));
        correction_factor = phi_tot / phi_tot_smooth;
        phi_new = phi_new * correction_factor;

    else
        phi_new = phi;
    end

end
```

D.5.3 k-ε model

```
function [nu_turb,k,eps] = k_epsilon(k,eps,U_jet,R,z,dt,i)

    % Eddy Viscosity
    C_mu = 0.09;
    nu_turb(i) = C_mu*k(i)^2/eps(i);

    % Velocity shear gradient
    du_jet_dr(i) = U_jet(i) / R(i);

    % k-epsilon model ------------------------------------------------------
    % k equation: Four terms, term 1: d/dz(nu_t dk/dz), term 2: 2 nu_t Eij,
    % term3: -epsilon, term4: d/dz(ku)

    LPfilter = 1e-3; % add a low pass filter to 1st term in both equations
    C = [1 1/1.3 1.44 1.92];

    if i > 2
        dk_dz(i) = C(1) * nu_turb(i)*(k(i) - k(i-1))/(z(i)-z(i-1));
        k_term1(i) = (dk_dz(i) - dk_dz(i-1))/(z(i)-z(i-1));

        k_term1(i) = LPfilter*k_term1(i) + (1-LPfilter)*k_term1(i-1);
    else
        k_term1(i) = 0;
    end
    k_term2 = 2*nu_turb(i)*(du_jet_dr(i) - k(i)/3);
    k_term3 = - eps(i);
    if i > 1
        k_term4(i) = -(k(i)*U_jet(i) - k(i-1)*U_jet(i-1))/(z(i)-z(i-1));
    else
        k_term4(i) = 0;
    end

    % numerically integrate
    dk_dt(i) = k_term1(i) + k_term2 + k_term3 + k_term4(i);
    k(i+1) = k(i) + dk_dt(i)*dt;
    % epsilon equation: Four terms, term 1: d/dz(nu_t deps/dz), term 2: 2 nu_t Eij
eps/k,
    % term3: -epsilon^2/k, term4: d/dz(eps u)
    if i > 2
        deps_dz(i) = nu_turb(i)* (eps(i) - eps(i-1))/(z(i)-z(i-1));
        eps_term1(i) = C(2) * (deps_dz(i) - deps_dz(i-1))/(z(i)-z(i-1));

        eps_term1(i) = LPfilter*eps_term1(i) + (1-LPfilter)*eps_term1(i-1);
    else
        eps_term1(i) = 0;
    end
    eps_term2 = C(3)*2*nu_turb(i)*(du_jet_dr(i) - k(i)/3)*eps(i)/k(i);
    eps_term3 = - C(4)*eps(i)^2/k(i);
    if i > 1
        eps_term4(i) = -(eps(i)*U_jet(i) - eps(i-1)*U_jet(i-1))/(z(i)-z(i-1));
    else
        eps_term4(i) = 0;
    end
    % numerically integrate
    deps_dt(i) = eps_term1(i) + eps_term2 + eps_term3 + eps_term4(i);
    eps(i+1) = eps(i) + deps_dt(i)*dt;
end
```

D.5.4 Variable timestep

```
function [dt2,eff_err] = variable_timestep(dt, phi_coarse,phi_fine, tol)
    eff_err = mean(sqrt((phi_coarse - phi_fine).^2),"all");
    dtx = [0.5 2]; % maximum/minimum amount dt will be multiplied by
    dt_lim = [1e-9 1e-0]; % absolute limits on dt
    dt2 =  0.99 * min(max(sqrt(tol/(eff_err)),min(dtx)),max(dtx)) * dt;
    dt2 = min(max(dt2 , min(dt_lim)), max(dt_lim));
end
```

C.5.4 Calculation of the jet radius

```
function R = jet_radius(phi,phi_sum0,r,centre_index)
    % Radius ------------------------------------------------------------
    % Calculate the effective radius of the concentration curve containing
    % 99.9% of the original volume of dye
    ii = 0;
    phi_sum = 0;
    phi_sum_max = 0.99*phi_sum0;
    while phi_sum < phi_sum_max % increment radius until > 99.9% of original dye
        ii = ii + 1;
        phi_sum =
sum(phi(centre_index:centre_index+ii).*abs(r(centre_index:centre_index+ii)));
    end
    % Calculate the under and overshoot so that the radius can be
    % interpolated between them
    dphi_sum_over = phi_sum - phi_sum_max;
    dphi_sum_under = sum(phi(centre_index:centre_index+ii-
1).*abs(r(centre_index:centre_index+ii-1))) - phi_sum_max;
    ratio_sum = abs(dphi_sum_under) / (abs(dphi_sum_over) + abs(dphi_sum_under));
    R = ratio_sum*r(centre_index+ii) + (1-ratio_sum)*r(centre_index+ii-1);
end
```

D.5.5 Forward Euler integrator

```
function phi2 = ForwardEuler(phi,dphi_dt,dt)
    % Forward Euler Integrator
    phi2 = phi + dphi_dt*dt;
end
```

D.5.6 Main loop

```
%% Initial Setup
% Which closure model to use?
closure = "k_epsilon";

% Temporal Conditions
dt = 1e-5; t_max = 15; timesteps = round(1 / dt); t = 0;

% Radial Conditions
R = zeros(1,timesteps); R(1) = 0.05; r_max = 0.5; dr = r_max/2e3;
r = (-r_max:dr:r_max); centre_index = find(r == 0);

% Displacement (Z) Conditions
U_jet = zeros(1,timesteps); U_jet(1) = 0.2; z = zeros(1,timesteps);
% Initial Concentration (phi) Curve
for i = 1:length(r)
    if abs(r(i)) < R(1)
        phi(i) = 1;
    else
        phi(i) = 0;
    end
end
phi = [phi; zeros(timesteps,length(r))];
phi_sum0 = sum(phi(1,:).*abs(r))/2; % Total quantity of dye

% Initial k-epsilon conditions
I_t = 0.035; C_mu = 0.09; L_t = 0.07*2*R(1); k = 3/2 * (U_jet(1) * I_t)^2;
eps = C_mu^(3/4) * k^(3/2) / L_t;

%% Calculation
disp('----- Started PDE Solver -----')
tic
i = 0;
while t < t_max

    i = i + 1;

    phi(i,:) = smoothing(r,phi(i,:),i,5,3); % Periodic smoothing

    if closure == "mixing_length"
        nu_turb(i) = mixing_length(U_jet(i),R(i));
    elseif closure == "k_epsilon"
       [nu_turb,k,eps] = k_epsilon(k,eps,U_jet,R,z,dt,i);
    end
    nu_t(i) = nu_turb(i);

    dphi_dt = diffusion_eq(r,dr,phi(i,:),nu_turb(i)); % Full step
    phi_coarse = ForwardEuler(phi(i,:),dphi_dt,dt);

    phi_fine_half = ForwardEuler(phi(i,:),dphi_dt,dt/2); % Double half step
    dphi_dt_half = diffusion_eq(r,dr,phi_fine_half,nu_turb(i));
    phi_fine = ForwardEuler(phi_fine_half,dphi_dt_half,dt/2);
    phi(i+1,:) = phi_fine;

    tol = 1e-9; % Adaptive timestep
    [dt,eff_err] = variable_timestep(dt, phi_coarse,phi_fine, tol);

    dt_save(i) = dt;
```

```
    % Radius, displacement and velocity
    R(i+1) = jet_radius(phi(i,:),phi_sum0,r,centre_index);
    z(i+1) = z(i) + U_jet(i)*dt;
    U_jet(i+1) = (R(i)/R(i+1)) * U_jet(i);

    % Mass Entrainment
    m_dot(i) = U_jet(i).*R(i).^2;

    t = t+dt;
    tlist(i) = t;

    if z(i) > 1.01 % break early if jet impinges on wall
        break
    end

    tclock = toc; % Display current solver progress
    if mod(round(tclock*1e3),1e2) == 0
        disp(['Progress: ' num2str(z(i)*100) '%, Clock time: ' num2str(tclock) 's,
Timestep: ' num2str(dt_save(i)*1000) 'e-3, Eff_err: ' num2str(eff_err*1e9) 'e-9'])
    end
end
disp('----- PDE Solver Complete -----')
% Truncate the output arrays so that they are all the same length
z = z(1:i);
R = R(1:i);
U_jet = U_jet(1:i);
```

Appendix E: Element Size vs Accuracy

Aside from the obvious differences in eddy length scales, reduced resolution simulations display other inaccuracies. The 64^3 simulation shows an unrealistic symmetry, and negligible Kelvin-Helmholtz instability, which greatly reduces the mass entrainment factor.

With increasing resolution, the axial velocity also reduces, as the increased entrainment of mass leads to a greater transfer of momentum from the jet to the quiescent fluid and into turbulent eddies.

As the resolution improves, the error bars decrease. This is because the error was based on varying the time over which the mean was taken, and the higher resolution mesh has fewer large eddies which cause fluctuations in the radius of the jet. It is unclear what the mass entrainment factor of a 1024^3 element mesh would be, although it is definitely in the region of 0.15-2.

Fig. 10: Concentration of passive scalar at t = 10s for a mesh size of (a) 64^3, (b) 128^3, (c) 256^3, (d) 512^3

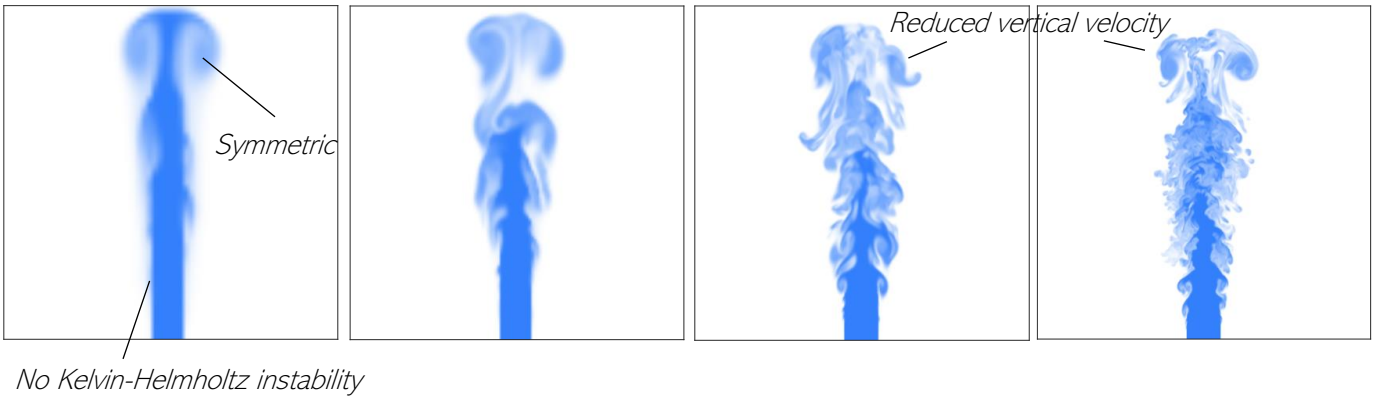

Fig. 11: Variation of mass entrainment factor for different mesh sizes. R_0 = 5cm, U_0 = 0.2m/s.